An Investigation of the Dependence of 3D Semi-Span Wing Behaviour on the Leading-edge Tubercles Configuration

Amgad Abdelkader[1], Abouelmagd Abdelsamie[2], Khairy Elsayed[2, 3]

[1]**Department of Mechanical Engineering, Faculty of Engineering and Technology, Badr University in Cairo, Badr City, Cairo, Egypt.**

[2]**Mechanical Power Engineering Department, Faculty of Engineering- Elmattaria, Helwan University, Cairo, Egypt.**

[3]**Mechanical Engineering Department, College of Engineering and Technology-Smart Village Campus, Arab Academy for Science, Technology and Maritime Transport, Giza, Egypt.**

Abstract:

Inspired by nature, experiments on the aerodynamic behavior of wings and wind turbines with sinusoidal leading-edge continued over the last two decades. The studies showed promising results at post-stall flow regimes as tubercles cause a more gradual lift loss and a higher stall angle of attack. This study aims to investigate numerically the dependence of the wing's aerodynamic coefficients on the tubercle's wavelength and amplitude at the stall angle of attack and 3D flow regime. The results show that increasing the tubercle's average amplitude up to 0.02 of the average chord increases the lift coefficient by 23.61% and decreases the drag coefficient by 4.61%. Similarly, decreasing the wavelength especially up to 1.1096 of the average chord increases the lift coefficient up to 21.55% and decreases the drag coefficient by 9.50%. Flow visualization shows that zones of attaching and separation flow form on the suction surface of the scalloped wings whereas the baseline wing is in a deep stall.

Keywords: Leading-edge tubercles; Computational fluid dynamics; Aerodynamics; Parametric study.

Abbreviation:

2D	two dimensional	$C_{L,\,max}$	maximum lift coefficient
3D	three dimensional	P1	amplitude design parameter

Amp	amplitude	C_L/C_D	lift to drag ratio
AoA	angle of attack [deg]	P2	wavelength design parameters
C_{avg}	Average chord	Re	Reynolds number [-]
C_L	lift coefficient	V	velocity [m/s]
C_D	drag coefficient	y+	non-dimensional distance

Greek letter

λ	Wavelength

1. Introduction

Over the last two decades, the aerodynamic behavior of wings and wind turbines with leading-edge tubercles was tested experimentally and numerically. Watts and fish [1] studied numerically a scalloped wing at the angle of attack (AoA) 10^o using the panel method and in 3D numerical code. Watts and Fish [1] found that the lift coefficient increased by 4.8%, and the lift to drag coefficient increased by 17.6% in the case of the scalloped wing. Watts and Fish [1] suggested that using tubercles would be more beneficial in AoAs larger than 15^o.

Miklosovic et al. [2] experimentally evaluated the aerodynamic coefficients for finite and infinite wings with and without tubercles. Miklosovic et al. [2] found that scalloped wings had a gentler stall behavior in both finite and infinite wings. Tubercles were more beneficial for the 3D wing. In contrast to the scalloped airfoil (2D), the scalloped 3D wing had a higher maximum lift coefficient and larger stall angle than the baseline wing. Miklosovic et al. [2], and Hansen et. al. [3] suggested that this flow behavior may be due to the change in local AoA. Although the change in local AoA creates a vortex-dominated flow, the results were not similar to wings with the traditional vortex generators [4]. Van Nierop et al. [5] stated that in contrast to tubercles the vortex generators' amplitude [4] is in order of magnitude of the boundary layer thickness.

Hansen et al. [3] studied the effect of tubercle's amplitude, wavelength, and amplitude to wavelength ratio on airfoils. Although wings with large amplitudes had a more gradual lift loss in the post-stall flow regime, wings with smaller amplitudes had a higher maximum lift coefficient. The baseline wing had the highest maximum lift coefficient. Reducing the wavelength for a certain point increased the maximum lift coefficient, and stall angle, and had a gentler lift loss. Nierop et al. [5] constructed a mathematical model to predict the influence of the tubercles on the wing's aerodynamic characteristics. Nierop et al. [5] found that as the tubercles amplitude increases the lift losses increase before the critical angle of attack. After the critical angle of attack, the stall became more gradual. The lift coefficient was insensitive to wavelength change.

Bolzon et al. [6] studied the effect of tubercles on swept wings at pre-stall flow regimes. Bolzon et al. [6] found that tubercles increase lift to drag coefficient (C_L/C_D) by reducing drag coefficient at angles of attack (AoAs) smaller than 8^o. for AoAs higher than 8^o, all aerodynamic coefficients were reduced as flow separates behind tubercles valleys.

Post et. al. [7] evaluated experimentally the aerodynamic coefficients of the baseline wing and five different scalloped wings. All scalloped wings had a gradual lift loss after stall. The scalloped wings with tubercles configuration similar to Hansen et al. [3] optimal design achieved the highest stall angle and best post-stall flow behavior. Straight wings achieved higher lift than swept wings. Post et al. [7] argued that by normalizing the area, the lift coefficient of the swept wings was higher than the straight wings. More research is needed on swept scalloped wings behavior.

Ibrahim et al. [8] compared a baseline wind turbine with slotted and scalloped wind turbines. The slotted wind turbine outperformed the baseline wind turbine at low wind speeds ($v \leq 6.5$ m/s). On the other hand, the scalloped wind turbine

had a better performance at high wind speed (v > 6.5 m/s) and under harsh weather conditions.

Abate et al. [9] tested the performance of wind turbines with different tubercles configurations and their effect on power and annual energy production. Abate et al. [9] found a considerable improvement for all tubercles configurations in high wind speeds and stall conditions. At low speed, tubercles degraded the wind turbine performance. Abate et al. [9] stated that tubercles generate counter-rotating vortices that prevent spanwise flow.

Ke et al. [10] investigated the influence of wind velocity on a sinusoidal leading-edge wind turbine. Ke et al. [10] found that tubercles were beneficial at off conditions and high wind velocity ($V \geq 7$ m/s), while tubercles degraded generated power at the on conditions and low wind speed ($V < 7$ m/s).

Lohry et al. [11] conducted a multi-objective optimization algorithm for the maximum lift coefficient (C_L) at angles of attack 14^o, and 20^o in an airfoil case. Lohry et al. [11] found that there is no single geometry that has optimum lift coefficient at both pre-stall and post-stall flow regimes. Lohry et al. [11] suggested that the tubercles serve as vertex generators. The improvement in the wing behavior is due to the interaction between the wing's tip vortex and leading-edge vortices.

Paula et al. [12] studied the effect of Reynold number (Re) on the baseline wing and on three scalloped wings with different leading-edge configurations (wings with tubercles at different amplitudes and wavelengths). Re ranged from 0.5×10^5 to 2.9×10^5. Paula et al. [12] found that the smallest amplitude and wavelength achieved the best performance between the four wings. The scalloped wing with the smallest amplitude and wavelength outperformed the baseline maximum lift coefficient by 19.4% and delayed the stall angle from AoA 10^o to 20^o at Re equals 1.2×10^5.

Lu et al. [13] optimized leading-edge tubercles geometry. The objective functions were delaying stall and increasing lift coefficient between AoAs 12^o and 16^o. Based on the Pareto front [14], four geometries were selected that achieve the two optimization objectives. Although the increase in lift coefficient between angles 12^o, and 16^o, the lift coefficient was smaller than the baseline wing for other angles of attack.

Cai et al. [15] studied the flow pattern around an airfoil at both the pre-stall and post-stall flow regimes. Cai et al. [15] found a periodic flow regime of flow separation behind valleys and attached flow behind peaks at small AoAs. After the stall angle of attack, an aperiodic and asymmetric flow pattern formed around the wings, as the flow separates only behind some valleys. The distance between the stalled valleys was stated to be 4-7 times the tubercles' wavelengths.

Custodio et al. [16] examined seven different wings with sinusoidal leading-edge protuberances in a water tunnel. Re ranged between 0.9×10^5 and 4.5×10^5. Custodio et al. [16] found Re number effect negligible beyond 3.6×10^5. Although the scalloped wings had a maximum lift coefficient equal to, or greater than the baseline wing, all scalloped wings had drag coefficients higher than the baseline wing.

Kim et al. [17] studied the influence of tubercles on wing behavior at Re equals 1.8×10^5. Tubercles delayed stall from AoA 8^o to 15^o and increased the maximum lift coefficient by 22%. Separation starts at the wings' tip for both the baseline and scalloped wings, but in the case of the scalloped wing, counter-rotating streamwise vortices served as a fence to prevent separation progression in a spanwise direction.

Wei et al. [18] investigated the performance of baseline and scalloped wings in a 3D flow regime. A scalloped wing achieved the highest stall angle, $C_{L,\,max}$, and max C_L/C_D coefficient. It has also a more gradual lift loss than the baseline wing. Wei et al. [18] stated that the scalloped wing's performance depends on the

tubercle's orientation relative to the flow direction. The scalloped wing had a higher C_D and lower lift/drag ratio than the baseline for almost all angles of attacks. Table 1 shows a brief description of the selected literature on the performance of the scalloped wings.

This study aims to investigate the impact of tubercles' amplitude and wavelength on the scalloped wing's lift, drag and lift to drag coefficients. The angle of attack 16^o was chosen for the analysis at the 3-D flow regime. The influence of sinusoidal leading-edge on the flow pattern around the wing would be also studied.

Table 1 Selected previous investigation of the aerodynamic performance of the scalloped wings and wind turbines.

Ref.	Exp. / Num.	Wing's Airfoil	2D / 3D	Re (X 10^5)	AoA (deg)	Observations
Watt & Fish [1]	Num.	NACA 63_4-021	2D	---	10^o	Scalloped wing had a 4.8% increase in lift, a 10.9% reduction in induced drag, and a 17.6% increase in the lift to drag ratio.
Miklosovic et al. [2]	Exp.	NACA 0020	2D 3D	2.74 5.34 – 6.31	0^o– 22^o	• Higher $C_{L,\ max}$ at the critical angle of attack. • a more gradual lift loss in the post-stall flow regime.
Hansen et al. [3]	Exp.	NACA 0021& NACA 65-021	2D	1.2	0^o– 25^o	• Lower $C_{L,\ max}$ than the baseline wing. • a more gradual lift loss in the post-stall flow field. • The optimum configuration has a small amplitude and small wavelengths.

Table 1 Selected previous investigation of the aerodynamic performance of the scalloped wings and wind turbines (continued).

Ref.	Exp. / Num.	Wing's Airfoil	2D / 3D	Re (X 10^5)	AoA (deg)	Observations
Bolzon [6]	Exp.	NACA 0021	3D	2.25	0^o-20^o	• For swept wings, tubercles reduced C_D and increased C_L/C_D for AoAs less than 8^o. • For larger AoAs, C_L and C_L/C_D are smaller than the baseline wing.
Post et al. [7]	Exp.	NACA 0020	3D	1.0 – 5.0	0^o-24^o	• The influence of the Reynolds number was negligible in the case of scalloped wings. • The stall was more gradual in the case of the scalloped wings.
Ibrahim et al. [8]	Exp.	NACA 4412	3D	----	----	• Tubercles delayed stall in the case of wind turbines and had a steadier response to wind speed change.
Abate et al. [9]	Num.	S809 (NREL VI wind turbine)	3D	U = 5, 10, 15, 20, 25 m/s	----	• The turbine's performance increases for small amplitude, large wavelength, and when only 5% or 38 % of the blade is covered with tubercles.

Table 1 Selected previous investigation of the aerodynamic performance of the scalloped wings and wind turbines (continued).

Ref.	Exp. / Num.	Wing's Airfoil	2D / 3D	Re (X 10^5)	AoA (deg)	Observations
Ke et al. [10]	Num.	S809 (NREL VI wind turbine)	3D	----	----	• For U <= 7 m/s, power generation degraded for scalloped wind turbines. • For U > 7 m/s, power generation increased for scalloped wind turbines.
Lohry et al. [11]	Num.	NACA 0020	2D	5.0	14^o & 20^o	• At AoA = 14^o, the baseline wing was the optimum configuration, whereas the large wavelength scalloped wings were the optimum configuration at AoA = 20^o.
Paula et al. [12]	Exp.	NACA 0030	2D	0.5 - 2.9	0^o- 30^o	• Small amplitude and small wavelength scalloped wing had $C_{L, max}$.
Cai et al. [15]	Exp.	NACA 63_4-021	2D	1.8	-15^o – 30^o	• Scalloped wings had a more gentle and stable stall behavior.
Custodio et al. [16]	Exp.	NACA 63_4-021	2D	0. 9 – 4.5	0^o- 30^o	• For scalloped wings, the Re effect was negligible for Re higher than 3.6 x 10^5. • Scalloped wings had C_D higher than the baseline wing so lower C_L/C_D.
Kim et al. [17]	Exp.	NACA 0020	3D	1.8	0^o – 25^o	• Tubercles delayed stall from AoA 8^o to 14^o. • Tubercles increased $C_{L, max}$ by 22%.
Wei et al. [18]	Exp.	SD7032	3D	2.2	-7^o – 29^o	• The scalloped wing has a higher stall angle of attack, $C_{L, max}$, and a more gradual stall behavior.

2. Methodology

2.1 Numerical Setup

The wings model is based on the geometry studied in both Ref. [2], and Ref. [7]. The wing geometry is based on the humpback whale flipper. The wing profile is NACA 0020 airfoil, and the equations for the original leading and trailing edges' profiles are

$$x_{LE} = 2.916 + 0.0624y + 0.000428y^2 - 0.000462y^3, \quad (1)$$

and

$$x_{TE} = \begin{cases} -3.152 - 0.113y + 0.0194y^2 - 0.000552y^3, & y \le 507\ mm \\ -0.374\sqrt{1 - 0.158(y - 19.98)^2} - 1.7, & 507\ mm < y \le 571 \text{ mm}. \end{cases} \quad (2)$$

The sinusoidal leading edge of the wing is presented as,

$$\Delta x_{LE} = 0.125(1 - 0.001y^2)\sin(0.57y^{1.5} - 0.4)\,(\tanh(y - 7) + 1). \quad (3)$$

The computational domain extends in every direction by five times the span except for the distance to the outlet which extends ten times the span. The mesh was generated using ANSYS Mesh. Inflation layers were created around the wing to achieve an average y+ less than one, so the buffer layer was avoided. An unstructured mesh of 6 million elements was used. The mesh has a skewness less than 0.85 and a minimum orthogonal quality higher than 0.01. The wing and the domain are shown in Figure 1.

The computational simulation was performed using ANSYS-Fluent at Re= 5.7 x 10^5. The transition SST turbulence model [19] was used. The transition SST turbulence model is a development of the k-ω SST turbulence model, and it's more suitable for the transitional flow regime as a part of the boundary layers is laminar. For the turbulent boundary layer, transition SST is reduced to k-ω SST. For the coupling between the pressure and velocity, The SIMPLEC algorithm was used with the second-order discretization. The boundary conditions were defined as velocity inlet, pressure outlet, and symmetry for the remaining boundaries.

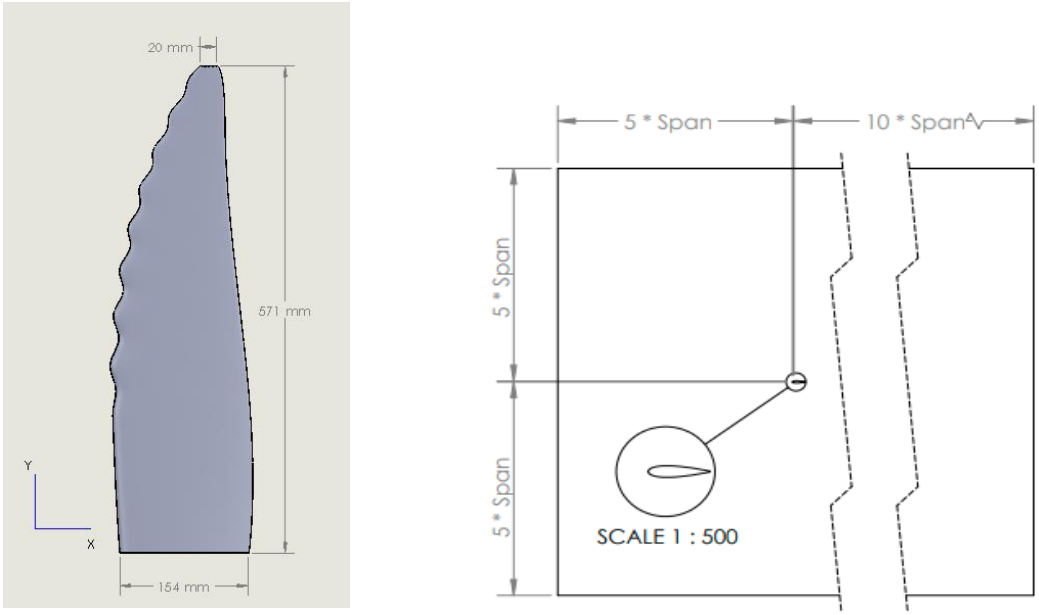

(a) (b)

Figure 1 Schematic drawing for the geometry and the domain. (a) The baseline wing, and (b) the domain.

The simulation was started as a steady-state simulation for faster conversion and after two hundred iterations, it was changed to an unsteady state simulation. The solver iterates in each time step until all residuals converge to less than 10^{-4} or a maximum number of iterations (50 iterations) is exceeded. The simulation stops when the fluctuation in the aerodynamic coefficients and y+ is less than 5% of the average.

Table 2 Mesh independence test.

Case No.	Elements Number	C_L/C_D	Error in C_L/C_D with respect to Ref. [7]
M1	4.6e5	13.3	-22.3%
M2	5.1e5	13.84	-19.2%
M3	5.6e5	14.9	-14.3%
M4	6.5e5	16.27	-5.1%
M5	7.3e5	16.86	-1.6%

2.2 Mesh independence test and validation

The experimental and numerical results of Ref. [7] were used for the validation of the numerical model. The grid dependence test was conducted at AoA 8^o similar to Ref. [7]. Five different mesh sizes were used in the mesh independence test, as shown in Table 2. The M4 mesh was chosen for the validation study as the error associated with the mesh is small and due to the limited computational cost. The validation showed a good agreement between the experimental results of Ref. [7] and the present study results. Table 3 summarizes the properties of the mesh used in the validation study.

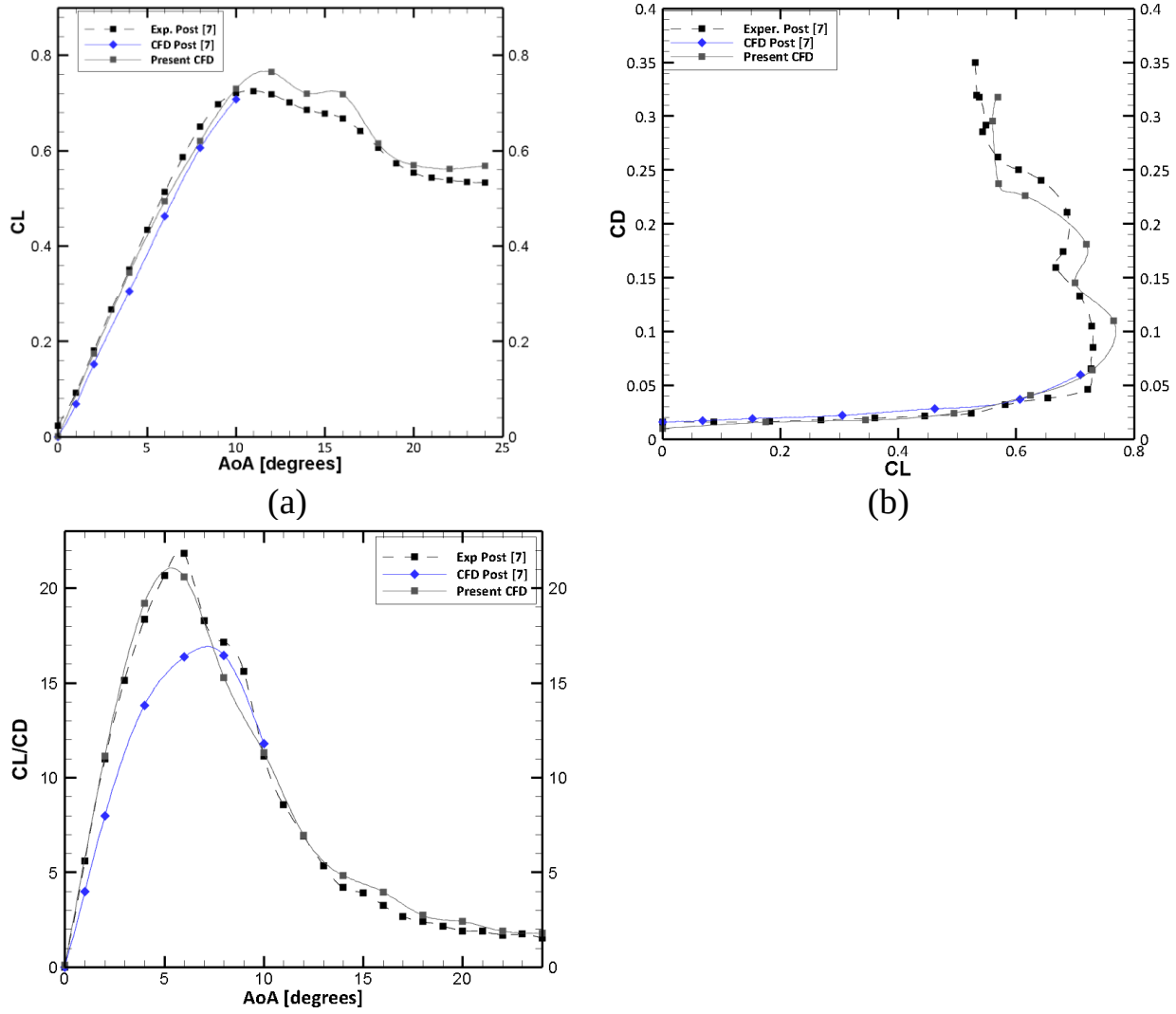

Figure 2 Validation of results with the Ref. [7] results for a. C_L coefficient, b. C_D coefficient, and c. C_L/C_D coefficient.

Table 3 Mesh Statistics

	Ansys Mesh Results	Recommended [20]
Y+	0.45	< 1
Max. Y+	3.1	< 5
Minimum Orthogonal Quality	0.02	> 0.01
Maximum Skewness	0.86474	< 0.95
Average Skewness	0.22	< 0.33
Maximum Aspect Ratio	840	< 1000
No. of Elements	5600 000	

2.3 Wings Models

Different scalloped wings with NACA 0020 cross-section profiles were evaluated and compared to the baseline wing. The amplitude and the wavelength were chosen as the design parameters. The wings configurations with their selected terminology are presented in Table 4, where $\overline{Amp}$ is the average amplitude, $\bar{\lambda}$ is the average wavelength, and C_{avg} is the average chord. P1 and P2 are the corresponding amplitude and wavelength parameters in Eq. 3, respectively. The wings models were named based on the approximated values of the two design parameters P1 and P2.

Table 4 Tubercle configurations.

Impact of the amplitude					Impact of the wavelength				
Wing Model	P1	$\frac{\overline{Amp}}{C_{avg}}$	P2	$\frac{\bar{\lambda}}{C_{avg}}$	Wing Model	P1	$\frac{\overline{Amp}}{C_{avg}}$	P2	$\frac{\bar{\lambda}}{C_{avg}}$
A0λ0	0	0	0	0	A0λ0	0	0	0	0
A03λ57	0.03125	0.0067	0.57	0.49	A12λ14	0.125	0.0267	0.1425	2.2192
A06λ57	0.0625	0.0134	0.57	0.49	A12λ28	0.125	0.0267	0.285	1.1096
A09λ57	0.09375	0.02	0.57	0.49	A12λ42	0.125	0.0267	0.4275	0.6340
A12λ57	0.125	0.0267	0.57	0.49	A12λ57	0.125	0.0267	0.57	0.49

3. Results and Discussion

In this section, the aerodynamic coefficients and flow visualization of the computational flow around the wings are shown. Figure 3 shows the dependence

of the three aerodynamic coefficients C_L, C_D, and C_L/C_D on tubercles' amplitude. The wings' performance depends greatly on the tubercle amplitude. For small amplitudes, the lift coefficient is approximately constant but with the increase of amplitude, C_L increases. The wing model A09λ57 achieved the highest lift coefficient and lift to drag ratio.

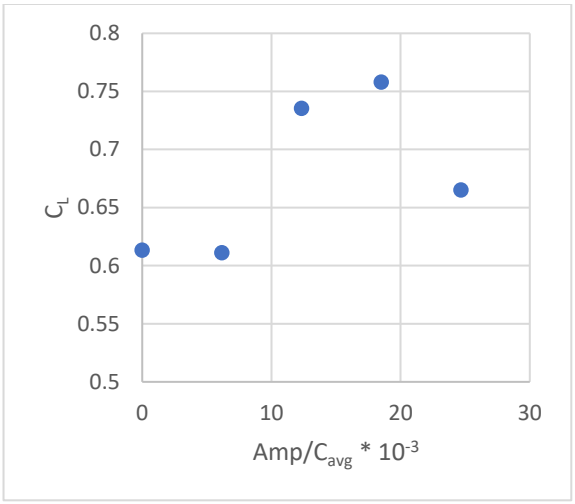

(a)

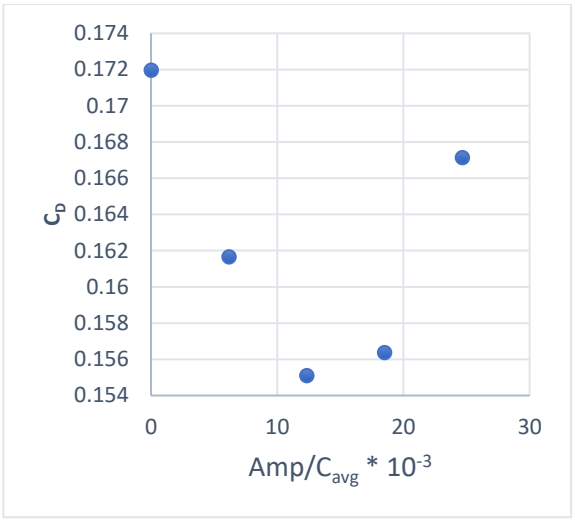

(b)

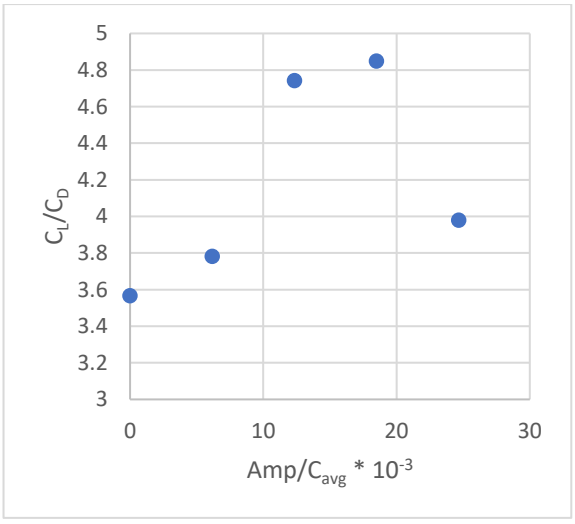

c

Figure 3 The dependence of aerodynamic coefficients on tubercle amplitude to the average chord at AoA 16º.

The percentage increase in C_L is 23.1 % by the baseline wing. This result is similar to the results obtained by Kim et al. [17]. The conclusion that the scalloped wing

has $C_{L,\,max}$ than the baseline wing was previously approved by Miklosovic et al. [2], Kim et al. [17], and Wei et al. [18].

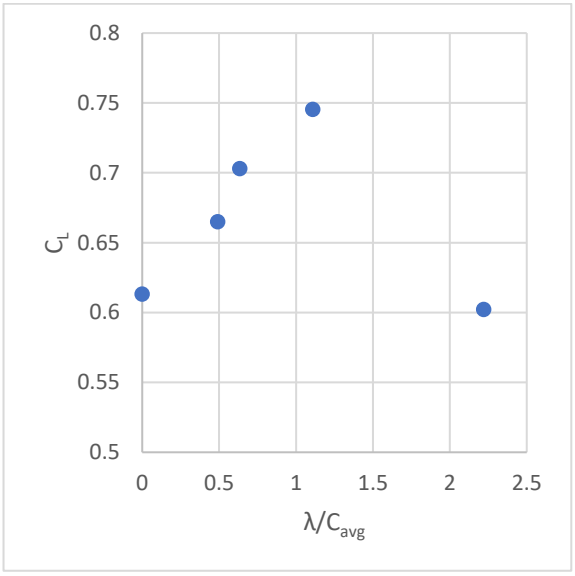

(a)

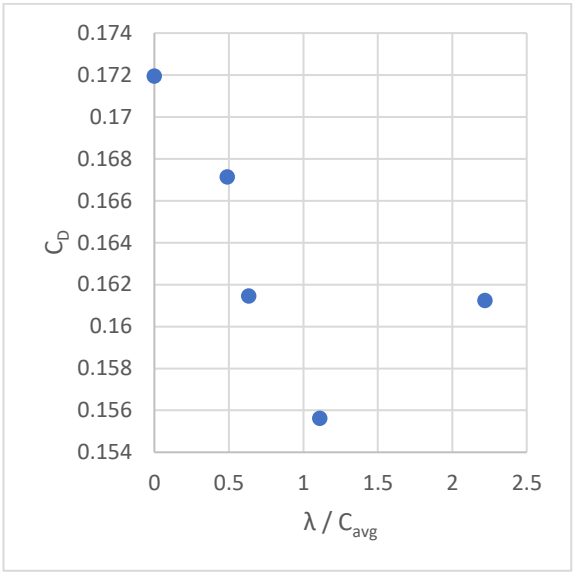

(b)

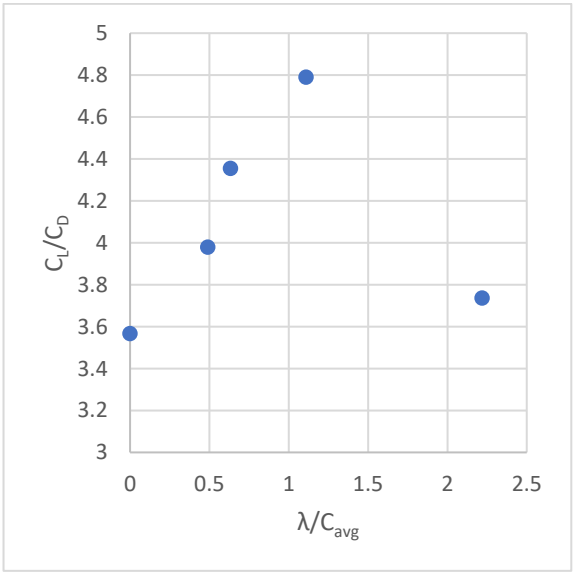

(c)

Figure 4 The dependence of aerodynamic coefficients on tubercle wavelength to the average chord at AoA 16º.

The C_D aerodynamic coefficient decreases with the increase in the amplitude parameter. The minimum drag coefficient is achieved by the A06λ57 wing. The A06λ57 wing has a smaller C_D than the baseline wing by 4.61%. The drag

increases for larger amplitudes. The baseline wing has the worst aerodynamic performance among all the wings as it has the minimum C_L -except for wing A03λ57- and the maximum C_D. As the increasing amplitude increases C_L and decreases C_D, the lift to drag coefficient increases with amplitude.

For the smallest amplitude, C_L/C_D is approximately horizontal. Afterward, C_L/C_D increases dramatically with the increase in amplitude. The maximum C_L/C_D is also achieved by the A09λ57 wing. The increase in C_L/C_D for the optimum configuration is 35.9%.

The wavelength parameter also greatly influences the wing performance, as shown in Figure 4. For large wavelengths and small tubercle fluctuations, there is a small performance degradation as it has a decrease in C_L coefficient by about -1.78%. Decreasing the wavelength, the lift increases largely as the maximum C_L is achieved by the A12λ28 wing. The increase in C_L is 21.6% more than the baseline wing. Any decrease in wavelength afterward decreases the lift coefficient.

The C_D coefficient decreases with the decrease in wavelength until the minimum C_D coefficient is also achieved by the A12λ28 wing. This wing has a drag coefficient less than the baseline wing by 9.5%. While amplitude increases the C_D greatly, the wavelength has a higher influence on the wavelength. Any further decrease in wavelength afterward increases the drag coefficient. Due to the behavior of the C_L and C_D coefficients, the wing with the largest wavelength (wing A12λ14) has the smallest C_L/C_D, even smaller than the baseline wing. Any further decrease in the wavelength increases the lift to drag coefficient until the maximum C_L/C_D is achieved by the A12λ28 wing. C_L/C_D decreases for smaller wavelengths.

Figure 5 shows the skin friction on the upper surface of the baseline and the A09λ57 wings. The zones of small skin friction coefficient indicate zones of stall flow. The figure shows that while the flow is completely stalled from the baseline surface, the flow remains attached to the wing A09λ57 surface behind the peaks.

Flow separates from the wing's surface behind tubercles valleys. Figure 6, and Figure 7 show the velocity contours around the A09λ57 wing at cross-sections located as illustrated on the wing scheme drawn on the upper right side of the figures.

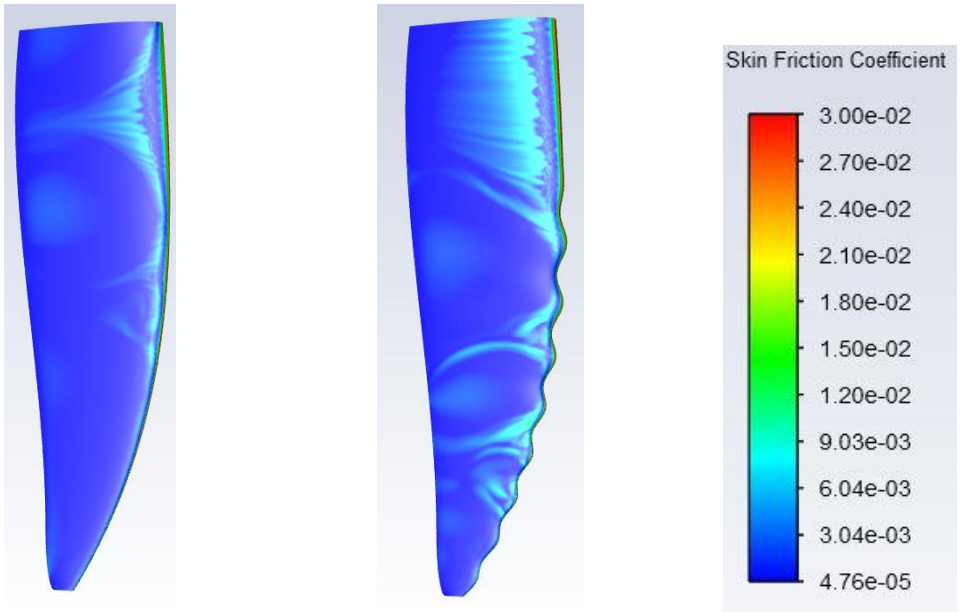

(a) (b)

Figure 5 Skin friction coefficient at the surface of the suction side of a. baseline wing, and b. A09λ57 wing at AoA 16°.

The flow separates from the wing's surface behind the tubercles valleys while remaining attached at the tubercles peaks. The flow downstream the valleys is energized by the attached flow at the tubercles' peaks. This causes the flow to re-attach to the wing's surface downstream several valleys, especially at the wing's mid-span. The fluid remains separated behind the other valleys and the separated flow propagates in a spanwise direction causing the flow to separate downstream from the neighboring peaks, as shown in Figure 5, Figure 6, and Figure 7. This flow pattern causes the formulation of attached and separated zones on the wing's surface.

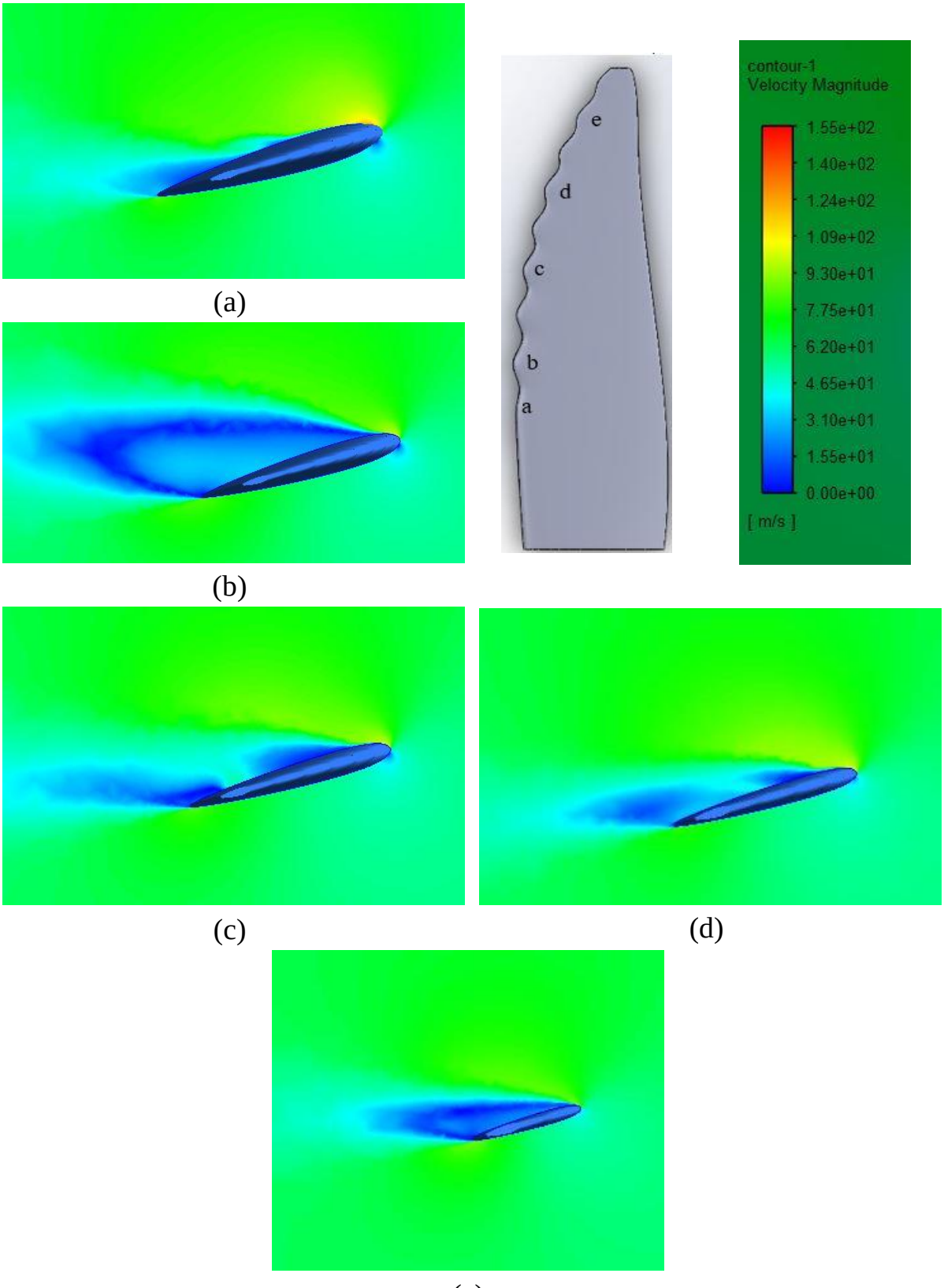

1 Figure 6 Velocity contours around the A09λ57 wing peaks at cross-sections
2 located at a, b, c, d, and e at AoA 16º.

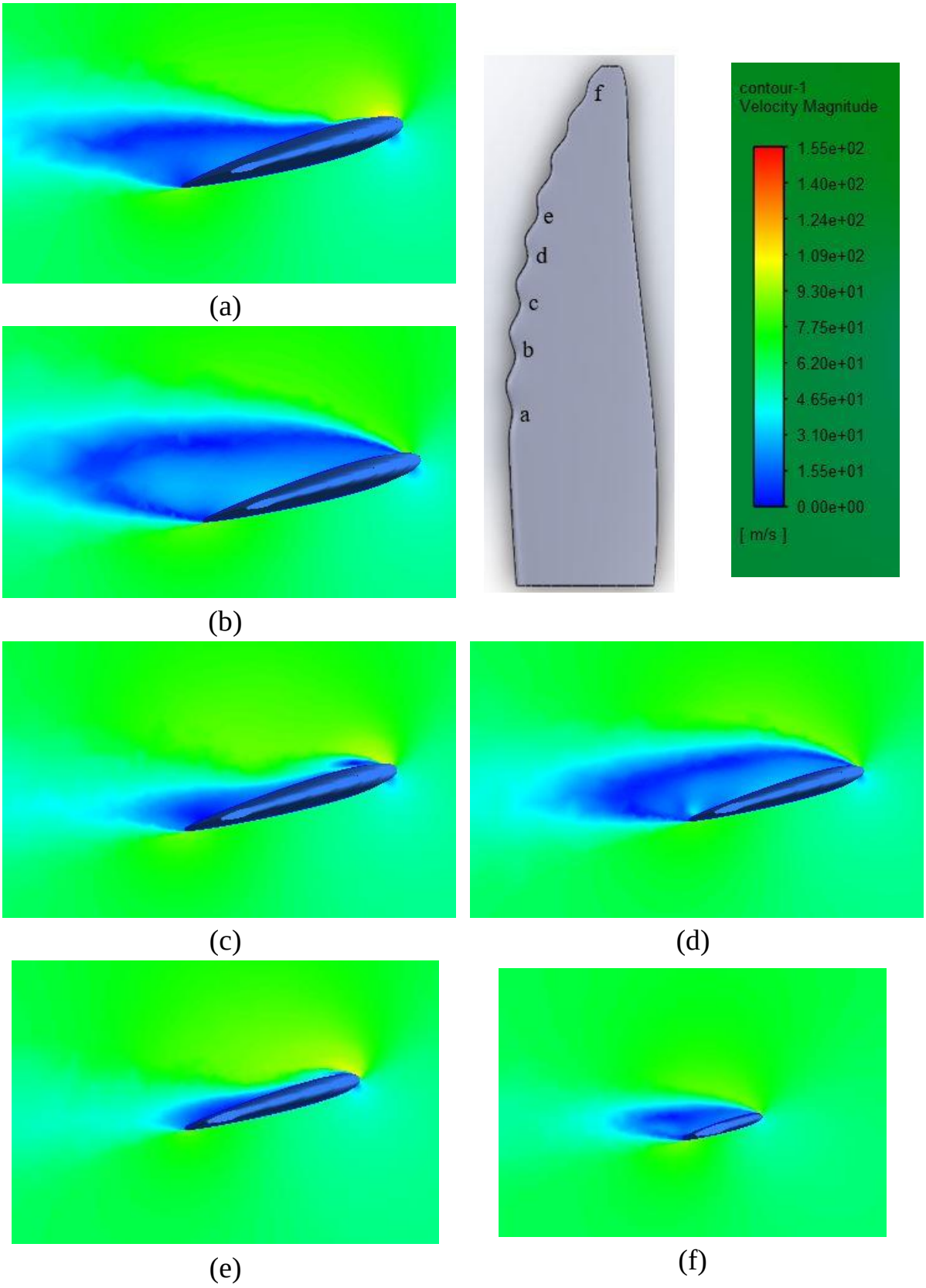

1 Figure 7 Velocity contours around the A09λ57 wing valleys at cross-sections
2 located at a, b, c, d, e, and f at AoA 16º.

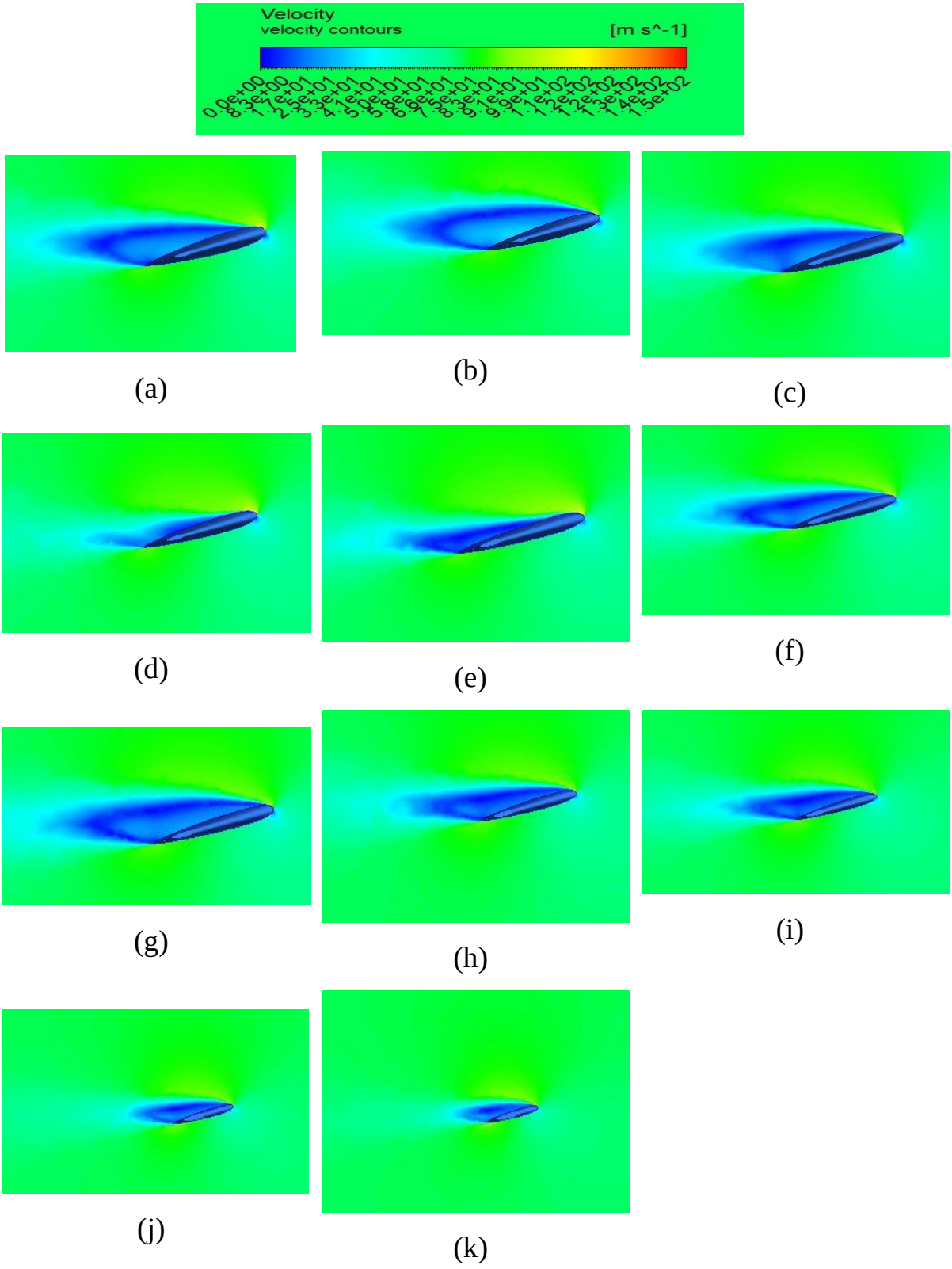

1 Figure 8 Velocity contours around the baseline wing at (a) 27.6%, (b) 33%, (c)
2 38.7%, (d) 44%, (e) 53.8%, (f) 58.2%, (g) 62.7%, (h) 71.1%, (i) 75%, (j) 90.2%,
3 and (k) 93.8% of the span from the wing's hub.

The baseline wing has the worst aerodynamic behavior among the tested wings. The flow fields around the baseline and scalloped wings cause the high performance of the scalloped wings in comparison to the baseline wing. Figure 8 shows the flow field around the baseline wing at the same positions as Figure 6, and Figure 7. Figure 8 shows that the flow is completely separated from the flow surface across the wing's chord, and at the different wing positions.

The study's results showed that the wings with small amplitude and large wavelength tubercles have a $C_{L,\,max}$ than the baseline wing at the baseline wing. Whereas Abate et al. [9], and Lohry et al. [11] results have an agreement with the study's optimum configuration, Hansen et al. [3], and Paula et al. [12] obtained a different optimum configuration of small amplitude and small wavelength. Further study is needed for the flow field structure and testing the performance of the optimum tubercles' configurations experimentally.

4. Conclusions

This study investigates the performance of wings with tubercles on the wing's leading edge and its dependence on the tubercle's amplitude and wavelength. The study found that the wing's performance greatly varies with the change of tubercle's amplitude and wavelength as

- Increasing amplitude increases the lift coefficient up to 23.61% and decreases the drag coefficient by 5.21% at mid-range amplitude. Any further increase in amplitude decreases lift and increases drag.
- Reducing wavelength also increases lift coefficient up to 21.55% and decreases drag coefficient by 9.50% in the case of mid-range wavelength. Any further reduction in wavelength decreases lift coefficient and increases drag coefficient.
- Flow visualization shows that the flow is completely separated from the upper surface of the baseline wing at the angle of attack 16^{o}.

- Flow visualization shows the formulation of attached and separated zones on the scalloped wings' surfaces. These zones cause the improvement in the wing's performance in the post-stall flow regime and the performance degradation in the pre-stall flow regime.

References

[1] P. Watts and F. E. Fish, "The Influence of Passive, Leading Edge Tubercles on Wing Performance," in *12th Internat Symp Unmanned Untethered Submersible Technology*, Durham, 2001.

[2] D. S. Miklosovic, M. M. Murray, and L. E. Howle, "Experimental Evaluation of Sinusoidal Leading Edges," *Journal oF Aircraft,* vol. 44, no. 4, pp. 1404-1407, 2007.

[3] K. L. Hansen, R. M. Kelso, and B. B. Dally, "Performance Variations of Leading-Edge Tubercles for Distinct Airfoil Profiles," *AIAA Journal,* vol. 49, no. 1, pp. 185-194, 2011.

[4] A. Jirasek, "Vortex-Generator Model and Its Application to Flow Control," *Journal of Aircraft,* vol. 42, no. 6, pp. 1486-1491, 2005.

[5] E. Van Nierop, S. Alben, and M. P. Brenner, "How Bumps on Whale Flippers Delay Stall: an Aerodynamic Model," *Physical Review Letters,* vol. 100, 2008.

[6] M. Bolzon, The Effects of Tubercles on Swept Wing Performance at Pre-Stall Angles of Attack. Ph. D., The University of Adelaide, 2017.

[7] M. Post, R. Decker, A. Sapell, and J. Hart, "Effect of Bio-Inspired Sinusoidal Leading-Edges on Wings," *Aerospace Science and Technology,* vol. 81, pp. 1-13, 2018.

[8] M. Ibrahim, A. Alsultan, S. Shen, and R. S. Aman, "Advances in Horizontal Axis Wind Turbine Blade Designs: Introduction of Slots and Tubercle," *Journal of Energy Resources Technology,* vol. 137, pp. 1-6, 2015.

[9] G. Abate, D. N. Mavris, and L. N. Sankar, "Performance Effects of Leading Edge Tubercles on the NREL Phase VI Wind Turbine Blade," *Journal Energy Resources Technology,* vol. 151, no. 5, 2019.

[10] W. Ke, I. Hashem, W. Zhang, and B. Zhu, "Influence of Leading-Edge Tubercles on the Aerodynamic Performance of a Horizontal-Axis Wind Turbine: A Numerical Study," *Energy*, vol. 239, no. B, 2022.

[11] M. W. Lohry, and L. Martinelli, "Genetic Algorithm Optimization of Periodic Wing Protuberances for Stall Mitigation," in *31st AIAA Applied Aerodynamics Conference*, San Diego, CA, 2013.

[12] A. A. d. Paula, J. R. Meneghini, V. G. Kleine, and R. d. M. Girard, "The Wavy Leading Edge Performance for a Very Thick Airfoil," in *55th AIAA Aerospace Sciences Meeting*, Grapevine, Texas, 2017.

[13] Lu, Z. Li, X. Chang, Z. Chuang, and J. Xing, "An Aerodynamic Optimization Design Study on the Bio-Inspired Airfoil with Leading-Edge Tubercles," *Engineering Applications of Computational Fluid Mechanics*, vol. 15, no. 1, pp. 293-313, 2021.

[14] P. Ngatchou, A. Zarei, and A. El-Sharkawi, "Pareto Multi Objective Optimization," in *Proceedings of the 13th International Conference on, Intelligent Systems Application to Power Systems*, 2005.

[15] Z. Z. Chang Cai, T. Maeda, Y. Kamada, Q. Li, K. Shimamoto, and S. Liu, "Periodic and Aperiodic Flow Patterns around an Airfoil with Leading-Edge Protuberances," *Physics of Fluids*, vol. 29, 2017.

[16] D. Custodio, C. W. Henoch, and H. Johari, "Aerodynamic Characteristics of Finite Span Wings with Leading-Edge Protuberances," *AIAA Journal*, vol. 53, no. 7, pp. 1878-1893, 2015.

[17] H. Kim, J. Kim, and H. Choi, "Flow Structure Modifications by Leading-Edge Tubercles on a 3D Wing," *Bioinspiration & Biomimetics*, vol. 13, no. 6, 2018.

[18] Z. Wei, T. H. New, and Y. D. Cui, "Aerodynamic Performance and Surface Flow Structures of Leading-Edge Tubercled Tapered Swept-Back Wings," *AIAA Journal*, vol. 56, no. 1, 2017.

[19] F. R. Menter, R. B. Langtry, S. R. Likki, Y. B. Suzen, P. G. Huang, and S. Volker, "A Correlation-Based Transition Model Using Local Variables: Part I — Model Formulation," in *ASME Turbo Expo*, Vienna, Austria, 2004.

[20] F. Goetten, D. Finger, M. Marino, C. Bil, M Havermann, and C. Braun, "A review of guidelines and best practices for subsonic aerodynamic simulations using RANS CFD," in *Asia Pacific International Symposium ON Aerospace Technology*, 2019.

[21] P. Ashill, J. Fulker and K. Hackett, "Research at DERA on Sub Boundary Layer Vortex Generators (SBVGs)," in *39th Aerospace Sciences Meeting and Exhibit*, Nevada, 2011.

1